UC Berkeley
UC Berkeley Previously Published Works

Title
Strong correlations and orbital texture in single-layer 1T-TaSe2

Permalink

Journal

ISSN

Authors
Chen, Yi
Ruan, Wei
Wu, Meng
et al.

Publication Date

DOI

Strong Correlations and Orbital Texture in Single-Layer 1T-TaSe₂

Yi Chen[1,2,†], Wei Ruan[1,2,†], Meng Wu[1,2,†], Shujie Tang[3,4,5,6,7,†], Hyejin Ryu[5,8], Hsin-Zon Tsai[1,9],

Ryan Lee[1], Salman Kahn[1], Franklin Liou[1], Caihong Jia[1,2,10], Oliver R. Albertini[11], Hongyu

Xiong[3,4], Tao Jia[3,4], Zhi Liu[6], Jonathan A. Sobota[3,5], Amy Y. Liu[11], Joel E. Moore[1,2], Zhi-Xun

Shen[3,4], Steven G. Louie[1,2], Sung-Kwan Mo[5], and Michael F. Crommie[1,2,12,*]

[1]Department of Physics, University of California, Berkeley, CA 94720, USA

[2]Materials Sciences Division, Lawrence Berkeley National Laboratory, Berkeley, California 94720, USA

[3]Stanford Institute for Materials and Energy Sciences, SLAC National Accelerator Laboratory and Stanford University, Menlo Park, CA 94025, USA

[4]Geballe Laboratory for Advanced Materials, Departments of Physics and Applied Physics, Stanford University, Stanford, CA 94305, USA

[5]Advanced Light Source, Lawrence Berkeley National Laboratory, Berkeley, CA 94720, USA

[6]CAS Center for Excellence in Superconducting Electronics, Shanghai Institute of Microsystem and Information Technology, Chinese Academy of Sciences, Shanghai 200050, China

[7]School of Physical Science and Technology, Shanghai Tech University, Shanghai 200031, China

[8]Center for Spintronics, Korea Institute of Science and Technology, Seoul 02792, South Korea

[9]International Collaborative Laboratory of 2D Materials for Optoelectronic Science & Technology of Ministry of Education, Engineering Technology Research Center for 2D Material Information Function Devices and Systems of Guangdong Province, Shenzhen University, Shenzhen 518060, China

[10]Henan Key Laboratory of Photovoltaic Materials and Laboratory of Low-dimensional Materials Science, School of Physics and Electronics, Henan University, Kaifeng 475004, China

[11]Department of Physics, Georgetown University, Washington, DC 20057, USA

[12]Kavli Energy Nano Sciences Institute at the University of California Berkeley and the Lawrence Berkeley National Laboratory, Berkeley, California 94720, USA

30 *† These authors contributed equally to this work.*

31 **e-mail: crommie@berkeley.edu*

32

33 **Abstract:**

34 Strong electron correlation can induce Mott insulating behavior and produce intriguing states of

35 matter such as unconventional superconductivity and quantum spin liquids. Recent advances in

36 van der Waals material synthesis enable the exploration of Mott systems in the two-dimensional

37 limit. Here we report characterization of the local electronic properties of single- and few-layer

38 1T-$TaSe_2$ via spatial- and momentum-resolved spectroscopy involving scanning tunneling

39 microscopy and angle-resolved photoemission. Our results indicate that electron correlation

40 induces a robust Mott insulator state in single-layer 1T-$TaSe_2$ that is accompanied by unusual

41 orbital texture. Interlayer coupling weakens the insulating phase, as shown by reduction of the

42 energy gap and quenching of the correlation-driven orbital texture in bilayer and trilayer 1T-

43 $TaSe_2$. This establishes single-layer 1T-$TaSe_2$ as a useful platform for investigating strong

44 correlation physics in two dimensions.

45

46   Two-dimensional (2D) Mott insulators emerge when the Coulomb interaction (U) exceeds

47   the bandwidth (W) in partially-filled band systems that can be described by 2D Hubbard-like

48   models[1]. Correlated electronic behavior in quasi-2D Mott insulators leads to collective quantum

49   phenomena[2,3] such as high-temperature superconductivity which is widely believed to arise

50   through doping of Mott insulating copper-oxygen layers[4,5]. Certain stacked graphene systems

51   have also recently been found to exhibit Mott-like insulating behavior and unconventional

52   superconductivity upon gating[6-9]. Layered transition metal dichalcogenides (TMDs) offer another

53   family of correlated quasi-2D materials, two examples being bulk $1T\text{-}TaS_2$ and the surface of

54   bulk $1T\text{-}TaSe_2$ which have long been known to host unusual insulating phases in the star-of-

55   David charge density wave (CDW) state[10-13]. Although widely believed to be Mott

56   insulators[11,14,15], the insulating nature of these bulk systems is complicated by interlayer CDW

57   stacking whose effects on the insulating phase remain controversial[16]. Interlayer hopping (which

58   increases W) and interlayer dielectric screening (which decreases U) are expected to suppress

59   Mott insulating behavior[1,17,18], but orbital stacking has also been predicted to open a

60   hybridization gap even in the absence of electron correlation[16,19,20].

61   Atomically-thin 1T-TMDs offer an ideal platform to differentiate the contributions of

62   electron correlation and interlayer effects in quasi-2D materials since single-layer systems can be

63   fully characterized in the absence of interlayer coupling. Without interlayer coupling the reduced

64   screening environment of a single-layer leads to increased Coulomb interaction and potentially

65   enhanced correlation phenomena[21-25]. The effects of interlayer coupling can then be

66   systematically determined by adding new layers to a material one at a time and mapping out the

67   resulting stacking order and wavefunction properties. Previous studies on single-layer $1T\text{-}NbSe_2$

68   and $1T\text{-}TaSe_2$ have found unusual insulating behavior[26,27], but electronic wavefunction texture

69   and interlayer coupling effects were not examined. The nature of the insulating phase in these

70   single-layer materials thus remains inconclusive.

71   Here we report a combined scanning tunneling microscopy/spectroscopy (STM/STS), angle-

72   resolved photoemission spectroscopy (ARPES), and theoretical study of the electronic structure

73   of single-layer $1T\text{-}TaSe_2$. Our results show that in the absence of interlayer coupling single-layer

74    $1T\text{-}TaSe_2$ hosts a Mott-insulating ground state that exhibits a 109 ± 18 meV energy gap and

75   unusual orbital texture. Bilayer and trilayer $1T\text{-}TaSe_2$ with shifted stacking order exhibit

76   successively smaller energy gaps and show no signs of the unusual orbital texture seen in the

77   single-layer limit. The single-layer band structure and density of states of $1T\text{-}TaSe_2$ are found to

78   be consistent with DFT+U calculations, confirming its Mott insulator nature. The unusual single-

79   layer orbital texture, however, is not captured by DFT+U, but is consistent with the behavior

80   expected for a weakly screened, strongly correlated 2D insulator. Reduction of the $1T\text{-}TaSe_2$

81   bandgap and quenching of the unusual orbital texture by the addition of new layers shows that

82   the effect of interlayer coupling on shifted-stacked $1T\text{-}TaSe_2$ is to weaken the Mott behavior.

83   The single-layer limit of $1T\text{-}TaSe_2$ is thus unique in that strong correlation effects here are most

84   pronounced, affecting both the energy gap and electron wavefunction symmetry.

85   **Electronic structure of single-layer $1T\text{-}TaSe_2$ in the CDW phase**

86   Our experiments were carried out on $1T\text{-}TaSe_2$ thin films grown by molecular beam epitaxy

87   on epitaxial bilayer-graphene-terminated (BLG) 6H-SiC(0001), as sketched in Fig. 1a. The

88   crystal structure of $1T\text{-}TaSe_2$ consists of a layer of Ta atoms sandwiched between two layers of

89   Se atoms in an octahedral coordination. Fig. 1b illustrates the hexagonal morphology of our 1T-

90    $TaSe_2$ islands, indicating high epitaxial growth quality. A triangular CDW superlattice is

91   observed on single-layer, bilayer, and trilayer $1T\text{-}TaSe_2$, as seen in Figs. 1b, c, and

92 Supplementary Fig. 1 where each bright spot corresponds to a star-of-David CDW supercell.

93 Fourier analysis of STM images (Supplementary Fig. 2) together with low-energy electron

94 diffraction patterns (Supplementary Fig. 3) confirm the formation of a $\sqrt{13} \times \sqrt{13}$ CDW in

95 single-layer 1T-TaSe$_2$, similar to the commensurate CDW phase of bulk 1T-TaSe$_2$ at $T < 473$ K[28]

96 (the atomic lattice and CDW superlattice are observed to have a relative rotation angle of

97 ~13.9°). Reflection high-energy electron diffraction patterns (Fig. 1e) and X-ray photoelectron

98 spectroscopy (Fig. 1f) show the structural and chemical integrity of our single-layer 1T-TaSe$_2$

99 samples (1T and 1H islands do coexist in our samples due to the metastability of 1T-TaSe$_2$

100 (Supplementary Fig. 4)).

101   We experimentally determined the electronic structure of single-layer 1T-TaSe$_2$ in the star-

102 of-David CDW phase using ARPES and STS. Figs. 2a and 2b show the ARPES spectra of

103 single-layer 1T-TaSe$_2$ for p- and s-polarized light, respectively, obtained at $T = 12$ K. At low

104 binding energies the single-layer 1T-TaSe$_2$ ARPES spectra show strongly diminished intensity at

105 all observed momenta, indicating insulating behavior (some ARPES intensity from coexisting

106 1H-TaSe$_2$ islands can be seen crossing E_F at $k \approx 0.5$ Å^{-1} (white dashed lines)[29]). The CDW

107 superlattice potential induces band folding into a smaller CDW Brillouin zone (Fig. 2b inset).

108 One such band can be seen in the ARPES spectrum for p-polarized light (Fig. 2a) which shows a

109 prominent flat band centered at $E - E_F \approx$ -0.26 eV within the first CDW Brillouin zone (black

110 dashed box). A more dispersive band can be resolved outside of the first CDW Brillouin zone

111 boundary (vertical dashed lines labeled A and B mark this boundary). These features have no

112 obvious photon-energy dependence (Supplementary Fig. 5) and are similar to bands observed by

113 ARPES at the surface of bulk samples of 1T-TaS$_2$[16,30] and 1T-TaSe$_2$[12]. For s-polarized light (Fig.

114   2b) the flat band is much less visible and a manifold of highly dispersive bands near the Γ-point

115   dominates the spectrum.

116   Our STM dI/dV spectrum (Fig. 3a (black curve)) confirms the insulating nature of single-

117   layer 1T-TaSe$_2$. The electronic local density of states (LDOS) reflected in dI/dV exhibits a

118   pronounced valence band peak at $V = $ -0.33 V (labeled V_1) while dropping steeply at higher

119   energy until reaching zero at $V \approx$ -0.05 V. The zero LDOS region bracketing the Fermi level

120   yields an energy gap of magnitude 109 ± 18 meV (see Supplementary Fig. 6 for gap

121   determination). The experimental LDOS does not rise again until a narrow conduction band peak

122   is observed centered at $V = 0.20$ V (labeled C_1) in the empty state regime. The LDOS drops to

123   zero again above the C_1 peak until higher-lying conduction band features are seen to rise at $V >$

124   0.45 V (e.g., C_2, C_3). Aside from spatial variation in the relative peak heights, this gapped

125   electronic structure is observed uniformly over the entire single-layer 1T-TaSe$_2$ surface

126   (Supplementary Fig. 7). No significant band-bending effects are observed for different tip-

127   sample separations (Supplementary Note 1 and Supplementary Figs. 8, 9). To test substrate

128   effects we also grew single-layer 1T-TaSe$_2$ on cleaved graphite (HOPG), which shows similar

129   STM spectra compared to single-layer 1T-TaSe$_2$/BLG (Supplementary Note 2 and

130   Supplementary Fig. 10). This indicates that the small increase in screening provided by HOPG[21]

131   (as shown by the slight downshift/upshift of empty-state/filled-state features in Supplementary

132   Fig. 10) does not significantly change the 1T-TaSe$_2$ behavior. We are so far unable to

133   experimentally test the effect of reducing screening below the level provided by BLG.

134   **Experimental orbital texture of single-layer 1T-TaSe$_2$**

135   To gain additional insight into the insulating ground state of single-layer 1T-TaSe$_2$, we

136   performed dI/dV spatial mapping of its energy-dependent orbital texture at constant tip-sample

137   separation (Figs. 3b-h). dI/dV maps measured at negative biases all display a similar pattern

138   where high-intensity LDOS is concentrated near the center of each star-of-David (Figs. 3b, c,

139   and Supplementary Fig. 11). The experimental empty-state LDOS of single-layer 1T-TaSe$_2$,

140   however, exhibits a completely different orbital texture. This is most clearly seen in the dI/dV

141   map taken at the lowest conduction band peak C_1 (Fig. 3d) where the center of each CDW

142   supercell is observed to be dark (i.e., no LDOS intensity). At this energy the LDOS exhibits an

143   unusual, interlocked "flower" pattern (circled by yellow dashed lines) consisting of six well-

144   defined "petals" (i.e., bright spots) located around the outer rim of each star-of-David. This

145   appearance is completely different from previous reports of conduction band LDOS in bulk 1T-

146   TaSe$_2$ and 1T-TaS$_2$[13,31] (which show LDOS concentrated in the star-of-David centers), and is

147   clearly not due to defects since it follows the CDW periodicity. The 6-fold petal structure has a

148   different symmetry than the 3-fold arrangement of top-layer Se atoms in the spaces between each

149   star-of-David, but it shares the 6-fold symmetry of the Ta atom arrangement (Fig. 3a inset and

150   Supplementary Fig. 12). Single-layer 1T-TaSe$_2$/HOPG shows a similar dI/dV map with the

151   dominant LDOS intensity located near the outer rim of the stars-of-David at the lowest

152   conduction band peak (dI/dV maps at other energies also look similar, see Supplementary Fig. 10

153   and Supplementary Note 2).

154   The dI/dV map of single-layer 1T-TaSe$_2$/BLG obtained at a slightly higher bias of $V = 0.6$ V

155   (C_2) show LDOS that is related to the flower pattern in that it exhibits a nearly *inverse* flower

156   (i.e., dark areas at C_1 are bright at C_2, see circled regions in Fig. 3e). At even higher energies the

157   single-layer 1T-TaSe$_2$ LDOS displays other intricate orbital textures. The map at 0.8 V (Fig. 3f),

158   for example, shows quasi-triangular patterns with intensity distributed near the outermost Ta C-

159   atoms (labeled according to the convention shown in Fig. 1d). This evolves into trimer-like

7

160   features at 1.1 V (Fig. 3g), and a network of "rings" with intensity near Ta B-atoms at $V = 1.2$ V

161   (Fig. 3h) (a complete set of constant-height dI/dV maps is shown in Supplementary Fig. 11).

162   To help quantify the complex energy-dependent LDOS distribution of single-layer 1T-TaSe$_2$,

163   we cross-correlated our dI/dV maps with a reference map taken at the maximum of the valence

164   band peak V_1 (Fig. 3c), which exhibits LDOS dominated by inner Ta A- and B-atoms. The

165   resulting cross-correlation values are color-coded in Fig. 3a and show that occupied states (-1V <

166    $V < 0$ V) all have a strong, positive cross-correlation (blue) with the valence band map at V_1 (i.e.,

167   the central Ta A- and B-atoms are bright at these energies and the C-atoms are darker). The

168   empty-state cross-correlation, however, is very different. At C_1 (where the flower pattern is

169   observed) the LDOS map is strongly anti-correlated (red) with the valence band map since the

170   LDOS here is dominated by Ta C-atoms. At slightly higher energy (C_2) the cross-correlation

171   flips to blue. This is due to the LDOS inversion that occurs at this energy (i.e., the inverse flower

172   pattern) which creates intensity at the interior A- and B-atoms. At higher energy the cross-

173   correlation flips again to red and stays red over a fairly wide energy range (~0.4 eV) before

174   flipping again to blue near C_3.

175

176   **Energy gap reduction and quenching of unusual orbital texture in few-layer 1T-TaSe$_2$**

177   We examined the effect of interlayer coupling on 1T-TaSe$_2$ by studying the evolution in

178   electronic structure as 1T-TaSe$_2$ is stacked layer by layer. We first determined the star-of-David

179   CDW stacking order for bilayer and trilayer 1T-TaSe$_2$. As seen in the STM images of Fig. 1b

180   and Supplementary Fig. 1, the CDW stacking order follows the shifted triclinic structure

181   whereby inner Ta "A-atoms" sit on top of outer Ta "C-atoms", similar to stacking observed in

182   bulk 1T-TaSe$_2$[32]. We observe that the energy gap for 1T-TaSe$_2$ narrows significantly when

8

183 interlayer coupling is added, as seen in the STM dI/dV spectra for bilayer and trilayer 1T-TaSe$_2$

184 shown in Fig. 4a. The bilayer energy gap reduces to 21 ± 8 meV while trilayer 1T-TaSe$_2$ shows a

185 reduction in LDOS at E_{F} that can be described as "semimetallic" but exhibits no true energy gap.

186 In addition to reducing the 1T-TaSe$_2$ energy gap, bilayer and trilayer formation also quench

187 the unusual orbital texture observed in the single-layer limit. As shown in the insets to Figs. 4b, c,

188 dI/dV maps of the lowest conduction band in bilayer and trilayer 1T-TaSe$_2$ show LDOS intensity

189 concentrated near the center of each star-of-David, in stark contrast to the flower-like orbital

190 texture observed in single-layer 1T-TaSe$_2$ at C_1. This difference can also be seen in the color-

191 coded cross-correlation values of bilayer and trilayer 1T-TaSe$_2$ (Figs. 4b, c). Using the valence

192 band LDOS shown in the insets as a reference (which is similar to the single-layer valence band

193 LDOS of Fig. 3c), the bilayer and trilayer cross-correlation remain strongly positive (blue)

194 throughout the lowest conduction band (thus emphasizing that the LDOS here is concentrated on

195 the interior Ta A- and B-atoms). The distinctive flower pattern seen in single-layer 1T-TaSe$_2$ at

196 C_1 (Fig. 3d) is never seen in bilayer or trilayer LDOS at any bias (Supplementary Figs. 13, 14).

197 **Theoretical electronic structure of single-layer 1T-TaSe$_2$ via DFT+U simulations**

198 There are two main physical questions that we seek to answer regarding our measurements

199 of single- and few-layer 1T-TaSe$_2$. First, what type of insulator is single-layer 1T-TaSe$_2$? And,

200 second, what is the effect of interlayer coupling on 1T-TaSe$_2$ electronic behavior as new layers

201 are added? To address these questions we first performed a conventional band structure

202 calculation for freestanding single-layer 1T-TaSe$_2$ using density functional theory (DFT). From

203 an intuitive perspective, single-layer 1T-TaSe$_2$ is expected to have metallic band structure since

204 there are an odd number of Ta ions in the star-of-David unit cell (13) and each Ta^{4+} ion has only

205 one d-electron (in principle substrate charge transfer could alter the electron counting and/or the

206   CDW behavior[33], but in our case charge transfer effects from the graphene substrate are

207   negligible (Supplementary Fig. 15 and Supplementary Note 3)). As expected, the DFT band

208   structure of single-layer 1T-TaSe$_2$ in the CDW phase calculated using the PBE exchange

209   correlation functional shows a metallic half-filled band at E_F (Supplementary Fig. 16). This

210   theoretical result, however, strongly disagrees with our experimental data which shows

211   insulating behavior for single-layer 1T-TaSe$_2$ (Figs. 2, 3). An explanation for this significant

212   discrepancy is that since the metallic band is so narrow (only ~20 meV wide) it is unstable to

213   splitting into lower and upper Hubbard bands (LHB and UHB) due to a high on-site Coulomb

214   energy (U) (i.e., the condition that causes Mott insulators to arise from otherwise metallic

215   phases)[1].

216   To test for Mott insulator formation in single-layer 1T-TaSe$_2$ we modeled the effects of

217   electron correlation by performing DFT+U simulations. We find that the DFT+U band structure

218   for a ferromagnetic ground state with $U = 2$ eV reproduces most of our experimentally observed

219   electronic structure for single-layer 1T-TaSe$_2$ (the DFT+U results were sensitive to neither the

220   magnetic ground state nor the structural optimization conditions, and our U value is consistent

221   with previous simulations of related systems[31,34,35] (see Supplementary Note 4 and

222   Supplementary Figs. 17-21)). The DFT+U band structure was first compared to our ARPES data

223   by unfolding it onto the Brillouin zone of an undistorted unit cell. As seen in Figs. 2c, d, and

224   Supplementary Fig. 22, it reproduces the gapped electronic structure and shows good overall

225   agreement with the ARPES spectra. In particular, DFT+U predicts that the LHB at -0.2 eV

226   originates mainly from Ta d_{z^2} orbitals, consistent with the higher ARPES intensity under p-

227   polarized light (Fig. 2a)[36].

228   The DFT+U simulations were also consistent with much of our STS data as shown in Fig. 5

229   which displays the simulated density-of-states spectrum and LDOS maps for single-layer 1T-

230   TaSe$_2$. The theoretical density-of-states spectrum (Fig. 5a (black line)) reproduces the dI/dV

231   spectrum (Fig. 3a) reasonably well in both the occupied and empty states. A LHB corresponding

232   to the experimental V$_1$ feature is seen, as well as an UHB corresponding to C$_1$, along with higher

233   energy features that correspond to the experimental C$_2$ and C$_3$ features. The orbital texture

234   generated by the DFT+U calculations (Figs. 5b-h) also agree well with the experimental dI/dV

235   maps in the valence band and upper conduction band regimes (i.e., the energies corresponding to

236   filled states and levels above C$_2$).

237   However, there are significant discrepancies between the experimental and theoretical

238   LDOS maps in the low-energy conduction band region ($0 < E \lesssim 0.6$ eV) where the unusual

239   orbital texture is observed experimentally. This is most clearly seen by comparing the theoretical

240   UHB LDOS map at 0.2 eV (Fig. 5d) with the experimental dI/dV map at $V = 0.2$ V (Fig. 3d) (i.e.,

241   the energy corresponding to C$_1$). The calculated LDOS has high intensity in the central Ta A-

242   and B-atom regions (similar to what is seen in the LHB) while the experiment shows the flower

243   pattern (i.e., the experimental LDOS occupies the Ta C-atom region and is dark in the central

244   area). There also exists significant disagreement at the next higher energy band feature (C$_2$), as

245   seen by comparison of Figs. 3e and 5e. Here the theoretical orbital texture (Fig. 5e) shows

246   propeller-like structures with no central LDOS, while the experimental dI/dV map (Fig. 3e)

247   shows an inverse of the C$_1$ flower pattern which has LDOS in the interior region of the star-of-

248   David (a complete set of theoretical LDOS maps is shown in Supplementary Fig. 23).

249   **Unusual empty-state orbital texture at C$_1$ and C$_2$**

250   The good agreement between our DFT+U simulations and the majority of our ARPES

251   and STM/STS data provides strong evidence that single-layer $1T\text{-}TaSe_2$ is a 2D Mott insulator.

252   However, the failure of the simulations to reproduce the unusual conduction band orbital texture

253   at C_1/C_2 implies that additional electron-electron interactions occur in single-layer $1T\text{-}TaSe_2$ that

254   are not captured by DFT+U. Electrons injected from the STM tip into single-layer $1T\text{-}TaSe_2$ at

255   the C_1/C_2 energies experience additional correlation effects originating from their Coulomb

256   interaction with electrons already present in the occupied electron states. Such behavior is

257   expected to arise due to the LHB charge distribution (Fig. 3c) which creates a spatially-varying

258   Coulomb repulsion landscape, $\tilde{U}(r)$, felt preferentially by electrons injected into UHB states

259   since they share a common orbital. $\tilde{U}(r)$ can be estimated by treating the LHB as a Gaussian

260   charge distribution within each star-of-David cluster and by calculating the resulting interaction

261   energy (Supplementary Note 5). This leads to a Coulomb landscape (Supplementary Fig. 24) that

262   is strongly repulsive to UHB electrons at the center of each star-of-David (where the LHB charge

263   density is large) and that has minima at precisely the locations of the six-fold C_1 flower petals

264   (where the LHB charge density is small). Given the composite nature of the UHB orbital (which

265   has contributions from 13 Ta atoms over the CDW cell) the unusual orbital texture at C_1/C_2 can

266   thus be understood as a redistribution of the UHB spectral density at the center of each star-of-

267   David up to higher energy in response to enhanced Coulomb interactions that arise from reduced

268   screening in 2D. The remaining state density of the composite UHB stays in the $\tilde{U}(r)$ minima

269   regions and gives rise to the peripheral six-fold C_1 flower petals. This picture is corroborated by

270   our observation that on the more strongly screened graphite substrate the LDOS distribution at

271   C_1 of single-layer $1T\text{-}TaSe_2$ appears to be more smeared out around the outer rim of the star-of-

272   David cells, consistent with a less corrugated $\tilde{U}(r)$ landscape (Supplementary Fig. 10 and

12

273 Supplementary Note 2). Future theoretical treatments considering dynamical interactions could

274 potentially provide more insight into this unusual strong correlation phenomenon.

275 The effect of interlayer coupling on the shifted-stacked 1T-TaSe$_2$ electronic structure is to

276 weaken the Mott insulator phase, both in view of the observed energy gap reduction with

277 increased layer number as well as its effect on orbital texture. The bilayer and trilayer orbital

278 textures, for example, show no signs of the correlation-induced spectral density shift seen in the

279 single-layer material at C$_1$/C$_2$. Such weakening of the Mott behavior likely arises from an

280 increase in the effective inter-star-of-David hopping parameter (t) of the bilayer and trilayer due

281 to interlayer coupling, as well as a reduction in Coulomb interactions due to increased electronic

282 delocalization and screening.

283 **Outlook**

284 We have shown that single-layer 1T-TaSe$_2$ is a strongly correlated 2D Mott insulator

285 characterized by unusual orbital texture. Interlayer coupling weakens the Mott behavior,

286 consistent with the evolution of 1T-TaSe$_2$ into a metal as its thickness is increased layer-by-layer.

287 The Mott insulator phase seen in single-layer 1T-TaSe$_2$ thus offers a highly-tunable 2D platform

288 for future exploration of metal-insulator transitions[1] where the Coulomb interaction might be

289 further modified by substrate screening[21,37], the bandwidth by pressure[38], or the carrier density by

290 electrostatic gating[6,8].

309 **Author contributions**

310 Y.C., W.R., and M.F.C. initiated and conceived the research. Y.C., W.R., H.-Z.T., R.L.,

311 S.K., F.L., and C.J. carried out STM/STS measurements and analyses. M.F.C supervised

312 STM/STS measurements and analyses. S.T., H.R., H.X., and T.J. performed sample growth and

313 ARPES measurements. S.-K.M., Z.-X.S., J.A.S., and Z.L. supervised sample growth and ARPES

314 measurements. M.W. performed DFT calculations and theoretical analyses. S.G.L. supervised

315 DFT calculations and theoretical analyses. J.E.M. performed electrostatic modeling. O.R.A. and

316 A.L. provided support for development of the CDW model. Y.C., W.R., and M.F.C. wrote the

317 manuscript with the help from all authors. All authors contributed to the scientific discussion.

318   **Competing interests**

319   The authors declare no competing interests.

320   **Data availability**

321   The data represented in Figs. 1f, 3a, 4, and 5a are available as source data in Supplementary

322   Data 1-4. All other data that support the plots within this paper and other findings of this study

323   are available from the corresponding author upon reasonable request.

324

325   **Code availability**

326   The codes used in this study are available from the corresponding author upon reasonable

327   request.

328

329   **Methods**

330   **Sample growth and ARPES measurements**

331   Single-layer 1T-TaSe$_2$ films were grown on epitaxial bilayer graphene terminated 6H-SiC(0001)

332   and cleaved HOPG substrates in a molecular beam epitaxy chamber operating at ultrahigh

333   vacuum (UHV, base pressure 2×10^{-10} Torr) at the HERS endstation of Beamline 10.0.1,

334   Advanced Light Source, Lawrence Berkeley National Laboratory. High purity Ta (99.9%) and

335   Se (99.999%) were evaporated from an electron-beam evaporator and a standard Knudsen cell,

336   respectively, with a Ta:Se flux ratio set between 1:10 and 1:20 and a substrate temperature of

337   660 $^{\circ}$C. A higher substrate temperature (compared with our previous 1H-TaSe$_2$ growth at 550

338   $^{\circ}$C[29]) was used to facilitate the growth of the metastable 1T phase of TaSe$_2$. The growth process

339   was monitored by reflection high-energy electron diffraction. After growth, the films were

340 transferred *in-situ* into the analysis chamber (base pressure 3×10^{-11} Torr) for ARPES and core-

341 level spectra measurements. The ARPES system was equipped with a Scienta R4000 electron

342 analyzer. The photon energy was set at 51 eV (unless specified otherwise) with energy and

343 angular resolution of 12 meV and 0.1°, respectively. *p*- and *s*-polarized light were used, as

344 described elsewhere (ref. [39]). Before taking the films out of vacuum for STM/STS measurements,

345 Se capping layers with ~10 nm thickness were deposited onto the samples for protection. These

346 were later removed by UHV annealing at ~200 $^{\circ}$C for 3 hours.

347 **STM/STS measurements**

348 STM/STS measurements were performed using a commercial CreaTec STM/AFM system at $T =$

349 5 K under UHV conditions. To avoid tip artifacts, STM tips were calibrated on a Au(111)

350 surface by measuring its herringbone surface reconstruction and Shockley surface state before all

351 STM/STS measurements. Both W and Pt-Ir STM tips were used and yielded similar results. STS

352 dI/dV spectra were obtained using standard lock-in techniques with a small bias modulation at

353 401 Hz. The constant-height mode (i.e., feedback loop open) was used for collecting all dI/dV

354 conductance maps. Before obtaining each set of maps the STM tip was parked near the sample

355 surface for at least 8 hours to minimize piezoelectric drift effects.

356 **Electronic structure calculations**

357 First-principles calculations of single-layer 1T-TaSe$_2$ were performed using density functional

358 theory (DFT) as implemented in the Quantum ESPRESSO package[40]. The onsite Hubbard

359 interaction was added through the simplified rotationally invariant approach using the same U

360 value for each Ta atom[41,42]. A slab model with 16 Å vacuum layer was adopted to avoid

361 interactions between periodic images. We employed optimized norm-conserving Vanderbilt

362 pseudopotentials (ONCVPSP) including Ta 5s and 5p semicore states (with a plane-wave energy

363 cutoff of 90 Ry)[43-45] as well as the Perdew-Burke-Ernzerhof (PBE) exchange-correlation

364 functional[46] in the generalized gradient approximation (GGA). The structure was fully relaxed at

365 the DFT-PBE level until the force on each atom was less than 0.02 eV/Å (unless specified

366 otherwise). The resulting relaxed single-layer 1T-TaSe$_2$ in the $\sqrt{13} \times \sqrt{13}$ CDW phase has a

367 lattice constant of $a = 12.63$ Å. Spin-orbit coupling was not taken into account in our calculations

368 since it has a negligible influence on the band structure given the inversion symmetry of this

369 system. The unfolding of the band structure from the CDW supercell to the undistorted unit cell

370 was calculated using the BandUP code[47,48] with band energies and wavefunctions obtained from

371 the Quantum ESPRESSO package.

372
373

References:

1   Imada, M., Fujimori, A. & Tokura, Y. Metal-insulator transitions. *Rev. Mod. Phys.* **70**, 1039-1263 (1998).

2   Keimer, B. & Moore, J. E. The physics of quantum materials. *Nat. Phys.* **13**, 1045-1055 (2017).

3   Kravchenko, S. *Strongly correlated electrons in two dimensions*. (Pan Stanford, 2017).

4   Dagotto, E. Correlated electrons in high-temperature superconductors. *Rev. Mod. Phys.* **66**, 763-840 (1994).

5   Lee, P. A., Nagaosa, N. & Wen, X.-G. Doping a Mott insulator: Physics of high-temperature superconductivity. *Rev. Mod. Phys.* **78**, 17-85 (2006).

6   Cao, Y. *et al.* Correlated insulator behaviour at half-filling in magic-angle graphene superlattices. *Nature* **556**, 80-84 (2018).

7   Cao, Y. *et al.* Unconventional superconductivity in magic-angle graphene superlattices. *Nature* **556**, 43-50 (2018).

8   Chen, G. *et al.* Evidence of a gate-tunable Mott insulator in a trilayer graphene moiré superlattice. *Nat. Phys.* **15**, 237-241 (2019).

9   Chen, G. *et al.* Signatures of tunable superconductivity in a trilayer graphene moiré superlattice. *Nature* **572**, 215-219 (2019).

10   Wilson, J. A. & Yoffe, A. D. The transition metal dichalcogenides discussion and interpretation of the observed optical, electrical and structural properties. *Adv. Phys.* **18**, 193-335 (1969).

11   Fazekas, P. & Tosatti, E. Electrical, structural and magnetic properties of pure and doped $1T$-TaS_2. *Philos. Mag. B* **39**, 229-244 (1979).

12   Perfetti, L. *et al.* Spectroscopic signatures of a bandwidth-controlled Mott transition at the surface of $1T$-$TaSe_2$. *Phys. Rev. Lett.* **90**, 166401 (2003).

13   Colonna, S. *et al.* Mott phase at the surface of $1T$-$TaSe_2$ observed by scanning tunneling microscopy. *Phys. Rev. Lett.* **94**, 036405 (2005).

14   Tosatti, E. & Fazekas, P. On the nature of the low-temperature phase of $1T$-TaS_2. *J. Phys. Colloq.* **37**, 165-168 (1976).

15   Sipos, B. *et al.* From Mott state to superconductivity in $1T$-TaS_2. *Nat. Mater.* **7**, 960-965 (2008).

16   Ritschel, T. *et al.* Orbital textures and charge density waves in transition metal dichalcogenides. *Nat. Phys.* **11**, 328-331 (2015).

17   Ma, L. *et al.* A metallic mosaic phase and the origin of Mott-insulating state in $1T$-TaS_2. *Nat. Commun.* **7**, 10956 (2016).

18   Cho, D. *et al.* Nanoscale manipulation of the Mott insulating state coupled to charge order in $1T$-TaS_2. *Nat. Commun.* **7**, 10453 (2016).

19   Ritschel, T., Berger, H. & Geck, J. Stacking-driven gap formation in layered $1T$-TaS_2. *Phys. Rev. B* **98**, 195134 (2018).

20   Lee, S.-H., Goh, J. S. & Cho, D. Origin of the Insulating Phase and First-Order Metal-Insulator Transition in $1T$-TaS_2. *Phys. Rev. Lett.* **122**, 106404 (2019).

21   Ugeda, M. M. *et al.* Giant bandgap renormalization and excitonic effects in a monolayer transition metal dichalcogenide semiconductor. *Nat. Mater.* **13**, 1091-1095 (2014).

22   He, K. *et al.* Tightly Bound Excitons in Monolayer WSe_2. *Phys. Rev. Lett.* **113**, 026803 (2014).

420 23 Qiu, D. Y., da Jornada, F. H. & Louie, S. G. Screening and many-body effects in two-
421   dimensional crystals: Monolayer MoS_2. *Phys. Rev. B* **93**, 235435 (2016).
422 24 Halperin, B. I. & Rice, T. M. Possible Anomalies at a Semimetal-Semiconductor
423   Transistion. *Rev. Mod. Phys.* **40**, 755-766 (1968).
424 25 Narozhny, B. N. & Levchenko, A. Coulomb drag. *Rev. Mod. Phys.* **88**, 025003 (2016).
425 26 Nakata, Y. *et al.* Monolayer $1T-NbSe_2$ as a Mott insulator. *NPG Asia Materials* **8**, e321
426   (2016).
427 27 Nakata, Y. *et al.* Selective fabrication of Mott-insulating and metallic monolayer TaSe2.
428   *ACS Appl. Nano Mater.* **1**, 1456-1460 (2018).
429 28 Di Salvo, F. J., Maines, R. G., Waszczak, J. V. & Schwall, R. E. Preparation and
430   properties of $1T-TaSe_2$. *Solid State Commun.* **14**, 497-501 (1974).
431 29 Ryu, H. *et al.* Persistent charge-density-wave order in single-Layer $TaSe_2$. *Nano Letters*
432   **18**, 689-694 (2018).
433 30 Sohrt, C., Stange, A., Bauer, M. & Rossnagel, K. How fast can a Peierls-Mott insulator
434   be melted? *Faraday Discuss.* **171**, 243-257 (2014).
435 31 Qiao, S. *et al.* Mottness collapse in $1T−TaS_{2−x}Se_x$ transition-metal dichalcogenide: an
436   Interplay between localized and itinerant orbitals. *Phys. Rev. X* **7**, 041054 (2017).
437 32 Brouwer, R. & Jellinek, F. The low-temperature superstructures of $1T-TaSe_2$ and 2H-
438      $TaSe_2$. *Physica B+C* **99**, 51-55 (1980).
439 33 Sanders, C. E. *et al.* Crystalline and electronic structure of single-layer TaS_2. *Phys. Rev.*
440   *B* **94**, 081404 (2016).
441 34 Darancet, P., Millis, A. J. & Marianetti, C. A. Three-dimensional metallic and two-
442   dimensional insulating behavior in octahedral tantalum dichalcogenides. *Phys. Rev. B* **90**,
443   045134 (2014).
444 35 Yu, X.-L. *et al.* Electronic correlation effects and orbital density wave in the layered
445   compound $1T-TaS_2$. *Phys. Rev. B* **96**, 125138 (2017).
446 36 Moser, S. An experimentalist's guide to the matrix element in angle resolved
447   photoemission. *J. Electron Spectrosc.* **214**, 29-52 (2017).
448 37 Qiu, Z. *et al.* Giant gate-tunable bandgap renormalization and excitonic effects in a 2D
449   semiconductor. *Sci. Adv.* **5**, eaaw2347 (2019).
450 38 Yankowitz, M. *et al.* Dynamic band-structure tuning of graphene moiré superlattices with
451   pressure. *Nature* **557**, 404-408 (2018).
452 39 Tang, S. *et al.* Quantum spin Hall state in monolayer $1T'-WTe_2$. *Nat. Phys.* **13**, 683-687
453   (2017).
454 40 Giannozzi, P. *et al.* QUANTUM ESPRESSO: a modular and open-source software
455   project for quantum simulations of materials. *J. Phys. Condens. Matter* **21**, 395502
456   (2009).
457 41 Liechtenstein, A. I., Anisimov, V. I. & Zaanen, J. Density-functional theory and strong
458   interactions: Orbital ordering in Mott-Hubbard insulators. *Phys. Rev. B* **52**, R5467-R5470
459   (1995).
460 42 Dudarev, S. L., Botton, G. A., Savrasov, S. Y., Humphreys, C. J. & Sutton, A. P.
461   Electron-energy-loss spectra and the structural stability of nickel oxide: An LSDA+U
462   study. *Phys. Rev. B* **57**, 1505-1509 (1998).
463 43 Hamann, D. R. Optimized norm-conserving Vanderbilt pseudopotentials. *Phys. Rev. B* **88**,
464   085117 (2013).

465 44 Schlipf, M. & Gygi, F. Optimization algorithm for the generation of ONCV
466   pseudopotentials. *Comput. Phys. Commun.* **196**, 36-44 (2015).
467 45 Scherpelz, P., Govoni, M., Hamada, I. & Galli, G. Implementation and Validation of
468   Fully Relativistic GW Calculations: Spin–Orbit Coupling in Molecules, Nanocrystals,
469   and Solids. *J. Chem. Theory Comput.* **12**, 3523-3544 (2016).
470 46 Perdew, J. P., Burke, K. & Ernzerhof, M. Generalized gradient approximation made
471   simple. *Phys. Rev. Lett.* **77**, 3865-3868 (1996).
472 47 Medeiros, P. V. C., Stafström, S. & Björk, J. Effects of extrinsic and intrinsic
473   perturbations on the electronic structure of graphene: Retaining an effective primitive cell
474   band structure by band unfolding. *Phys. Rev. B* **89**, 041407 (2014).
475 48 Medeiros, P. V. C., Tsirkin, S. S., Stafström, S. & Björk, J. Unfolding spinor wave
476   functions and expectation values of general operators: Introducing the unfolding-density
477   operator. *Phys. Rev. B* **91**, 041116 (2015).
478
479

480 **Fig. 1. Structure of single-layer 1T-TaSe$_2$ in the star-of-David CDW phase. a**, Top and side

481 view sketches of single-layer 1T-TaSe$_2$, including substrate. Clusters of 13 Ta atoms in star-of-

482 David CDW supercells are outlined, as well as the CDW unit cell. **b**, Large-scale STM

483 topograph of a typical 1T-TaSe$_2$ island shows monolayer and bilayer regions (V_b = -0.5 V, I_t = 10

484 pA, T = 5 K). **c**, A close-up STM image of single-layer 1T-TaSe$_2$. Each bright spot corresponds

485 to a star-of-David supercell (V_b = -0.17 V, I_t = 3 nA, T = 5 K). Black and orange parallelograms

486 mark CDW and atomic unit cells, respectively. **d**, Labels for Ta atoms in the star-of-David CDW

487 supercell depend on radial distance from center. **e**, Reflection high-energy electron diffraction

488 pattern of a submonolayer 1T-TaSe$_2$ film. **f**, X-ray photoelectron spectroscopy shows

489 characteristic peaks of Ta and Se core levels for a submonolayer 1T-TaSe$_2$ film.

490

Fig. 2. ARPES and DFT+U band structure of single-layer 1T-TaSe₂. ARPES spectra of single-layer 1T-TaSe₂ acquired with **a,** p- and **b,** s-polarized light at $T = 12$ K along the Γ-K' and Γ-M' directions defined in the undistorted (i.e., no CDW) unit cell Brillouin zone (yellow hexagon in Fig. 2b inset). ARPES spectra have little intensity at low binding energies except for coexisting 1H-TaSe₂ bands that cross E_F at $k \approx 0.5$ Å⁻¹ (white dashed lines). A strong flat band is seen under p-polarized light in the first CDW Brillouin zone (black dashed box in **a**). The full CDW Brillouin zone is sketched in the inset of **b** (black hexagon). **c**, DFT+U band structure ($U = 2$ eV) of single-layer 1T-TaSe₂ unfolded onto the undistorted unit cell Brillouin zone compared to ARPES spectrum under p-polarized light (from **a**). **d**, Same DFT+U band structure as in **c** compared to ARPES spectrum under s-polarized light (from **b**).
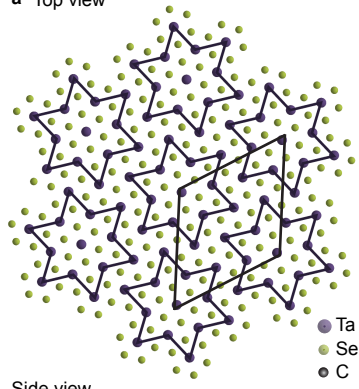
503 **Fig. 3. Experimental energy-resolved unusual orbital texture of single-layer 1T-TaSe$_2$. a**,

504 STS dI/dV spectrum of single-layer 1T-TaSe$_2$ shows a full energy gap bracketed by two STS

505 peaks labeled V$_1$ and C$_1$ (f = 401 Hz, I_t = 50 pA, V_{RMS} = 20 mV). Color shows cross-correlation

506 of dI/dV maps at different energies with the reference map shown in **c**. Inset shows how the

507 unusual orbital texture in **d** compares to atomic site locations (the 6-fold petal structure is shaded

508 gray in the inset). **b-h**, Constant-height dI/dV conductance maps of the same area for different

509 bias voltages show energy-dependent orbital texture (f = 401 Hz, V_{RMS} = 20 mV). The same star-

510 of-David CDW supercell is outlined in each map (orange line). Yellow dashed circles in **d**, **e**

511 highlight the unusual LDOS patterns at C$_1$ and C$_2$ and their relative spatial inversion.
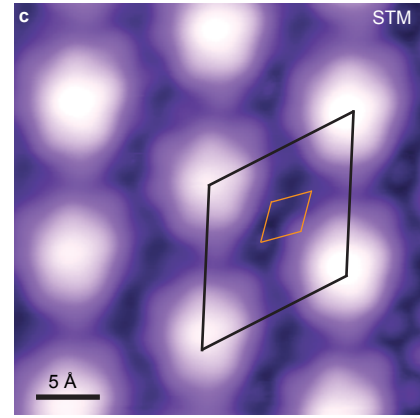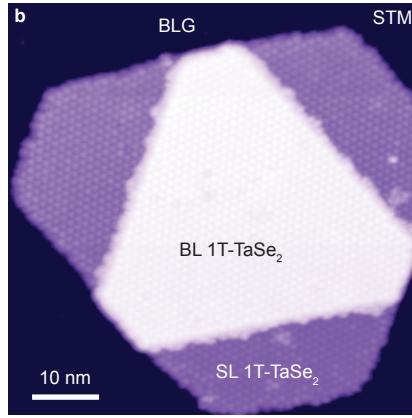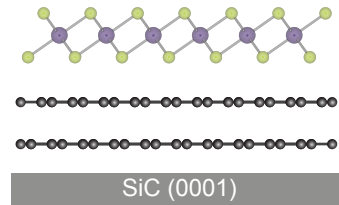
512

513   **Fig. 4. Energy gap reduction and quenching of unusual orbital texture in few-layer 1T-**

514   **TaSe$_2$. a**, STS dI/dV spectra for single-layer, bilayer, and trilayer 1T-TaSe$_2$ show how interlayer

515   coupling reduces the energy gap with an increasing number of layers. Spectra are shifted

516   vertically for viewing (horizontal dashed lines mark dI/dV = 0, f = 401 Hz, V_{RMS} = 2 mV). dI/dV

517   maps of the valence and conduction band LDOS as well as larger energy-scale dI/dV spectra of

518   **b,** bilayer, **c,** trilayer 1T-TaSe$_2$ (f = 401 Hz, V_{RMS} = 20 mV). Spatial cross-correlation values are

519   shown color-coded with references taken near the LDOS maximum of the valence band for

520   bilayer and trilayer 1T-TaSe$_2$. In contrast to single-layer 1T-TaSe$_2$, the lowest conduction band

521   for both bilayer or trilayer show no unusual orbital texture, thus resulting in positive cross-

522   correlation values (blue), indicating that LDOS is concentrated on the interior Ta A- and B-

523   atoms.

524

525

526   **Fig. 5. Theoretical orbital texture of single-layer 1T-TaSe$_2$ from DFT+U simulations. a,**

527   Theoretical density of states of single-layer 1T-TaSe$_2$ from DFT+U simulations ($U = 2$ eV).

528   Color shows cross-correlation of LDOS maps at different energies with respect to the reference

529   map in **c** (-0.2 eV). **b-h**, Theoretical LDOS maps of single-layer 1T-TaSe$_2$ from DFT+U

530   simulations ($U = 2$ eV). The same star-of-David supercell is outlined in each map (orange line).

531   Yellow dashed circles in **d**, **e** highlight two star-of-David clusters which show very different

532   theoretical conduction band orbital texture compared to experimental C$_1$ and C$_2$ features in Figs.

533   3d, e.

a Top view

Ta
Se
C

Side view

SiC (0001)

b BLG
BL 1T-TaSe$_2$
SL 1T-TaSe$_2$
STM
10 nm

c STM
5 Å

d
C
C
B B
C B A B C
B B
C C
C

e TaSe$_2$
graphene
RHEED

f XPS core level spectrum
$3d_{3/2}$
$3d_{5/2}$
Se
Ta
$5p_{3/2}$
$4f$ levels
Intensity (a.u.)
$E-E_F$ (eV)

a — M' A Γ B K'

ARPES *p*-polarization

$E - E_F$ (eV)

1T phase

1H phase

k_y (Å⁻¹) k_x (Å⁻¹)

High / Low

b — M' A Γ B K'

ARPES *s*-polarization

$E - E_F$ (eV)

k_y (Å⁻¹) k_x (Å⁻¹)

M' A M K' B K

k_y k_x

High / Low

c — M' A Γ B K'

Overlay of DFT+U on **a**

$E - E_F$ (eV)

k_y (Å⁻¹) k_x (Å⁻¹)

High / Low

d — M' A Γ B K'

Overlay of DFT+U on **b**

$E - E_F$ (eV)

k_y (Å⁻¹) k_x (Å⁻¹)

High / Low

b d*I*/d*V* (-0.6 V)
1 nm
EXPERIMENT

0 ——— max

a STS
Single-layer
1T-TaSe$_2$
Experiment
Cross-correlation

Top Se
Ta

V$_1$
C$_1$
C$_2$
C$_3$

d*I*/d*V* (a.u.)
Bias voltage (V)

h 1.2 V

0 ——— max

c -0.33 V
Ref

d 0.2 V

e 0.6 V

f 0.8 V

g 1.1 V

b LDOS(-0.6 eV)   1 nm   THEORY

a DFT+U, U = 2 eV
Single-layer
1T-TaSe$_2$

Theory

Density of states (a.u.)

Cross-correlation

Energy (eV)

0   max

h 1.0 eV

0   max

c -0.2 eV Ref

d 0.2 eV

e 0.4 eV

f 0.65 eV

g 0.9 eV